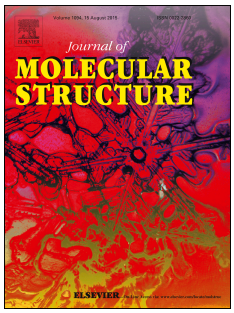

Biofilm inhibition and DNA binding studies of isoxazole-triazole conjugates in the development of effective anti-bacterial agents

Farhat Habib, Shadab Alam, Afzal Hussain, Babita Aneja, Mohammad Irfan, Mohamed F. Alajmi, Phool Hasan, Parvez Khan, Md Tabish Rehman, Omar Mohammed Noman, Amir Azam, Mohammad Abid

PII: S0022-2860(19)31253-0

DOI: https://doi.org/10.1016/j.molstruc.2019.127144

Reference: MOLSTR 127144

To appear in: *Journal of Molecular Structure*

Received Date: 27 June 2019

Revised Date: 16 September 2019

Accepted Date: 27 September 2019

Please cite this article as: F. Habib, S. Alam, A. Hussain, B. Aneja, M. Irfan, M.F. Alajmi, P. Hasan, P. Khan, M.T. Rehman, O.M. Noman, A. Azam, M. Abid, Biofilm inhibition and DNA binding studies of isoxazole-triazole conjugates in the development of effective anti-bacterial agents, *Journal of Molecular Structure* (2019), doi: https://doi.org/10.1016/j.molstruc.2019.127144.

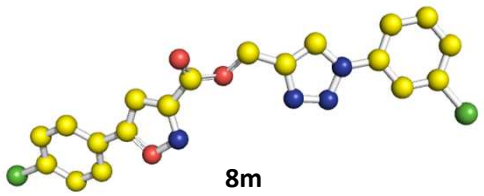

8m

Strain	IC_{50} in µg/mL
E. coli	83.17
S. pneumoniae	74.13
E. faecalis	44.66

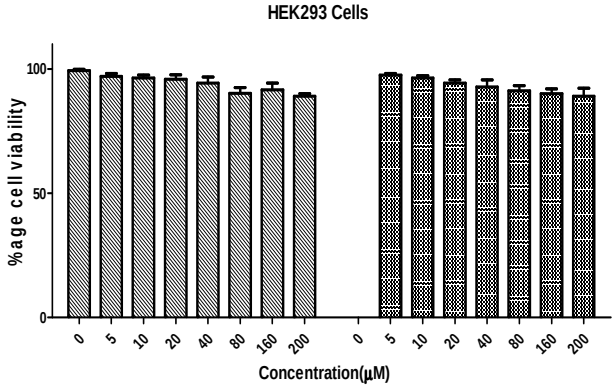

Cytotoxicity

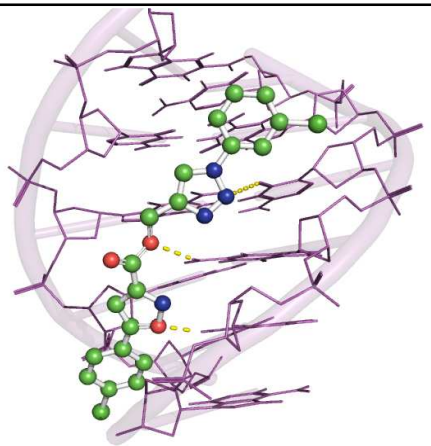

Docking studies

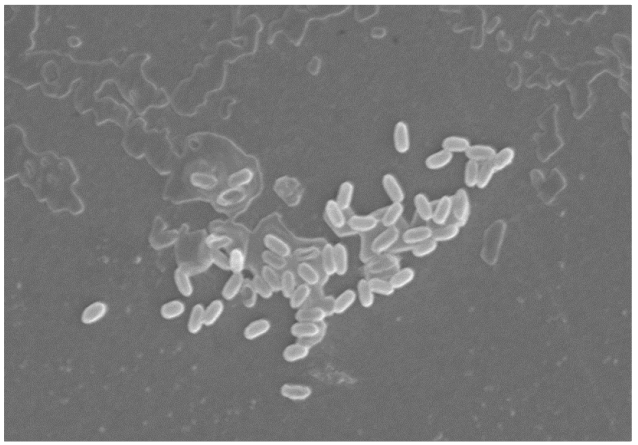

Biofilm inhibition

Biofilm inhibition and DNA binding studies of isoxazole-triazole conjugates in the development of effective anti-bacterial agents

Farhat Habib[a,b], Shadab Alam[a], Afzal Hussain[c], Babita Aneja[a,b], Mohammad Irfan[a], Mohamed F. Alajmi[c], Phool Hasan[a], Parvez Khan[d], Md Tabish Rehman[c], Omar Mohammed Noman[e], Amir Azam[b*], Mohammad Abid[a]

[a]*Medicinal Chemistry Laboratory, Department of Biosciences, Jamia Millia Islamia, New Delhi-110025, India.*

[b]*Department of Chemistry, Jamia Millia Islamia, New Delhi-110025, India.*

[c]*Department of Pharmacognosy College of Pharmacy, King Saud University, Riyadh, 11451, Kingdom of Saudi Arabia*

[d]*Centre for Interdisciplinary Research in Basic Science, Jamia Millia Islamia, New Delhi-110025, India.*

[e]*Medicinal, Aromatic and Poisonous Plants Research Center, College of Pharmacy, King Saud University, Riyadh-11451, Kingdom of Saudi Arabia.*

Corresponding author

M. Abid: mabid@jmi.ac.in; Tel: +91-8750295095

Co-corresponding author

A. Azam: amir_sumbul@yahoo.co.in; Tel: +91-9818963639

Abstract

Isoxazole-triazole conjugates (**8a-q**) were synthesized using click chemistry approach and their biological activities were explored to develop novel antibacterial agents. *In vitro* antibacterial screening against Gram-positive as well as Gram-negative bacterial strains identified compounds **8b** and **8m** with potent inhibitory potential against selective bacterial cells. **8b** showed IC_{50} value of 67.6 µg/mL against *P. aeruginosa* while **8m** exhibited better activity against Gram-positive bacteria *S. pneumoniae* and *E. faecalis* having IC_{50} values 74.13 and 44.7 µg/mL, respectively. Effect on growth kinetics of the bacterial cells as well as cytotoxicity studies on human embryonic kidney cells (HEK293) further supports their biological potential. Compound **8m** significantly inhibited biofilm formation of *E. coli* cells visualized by scanning electron microscopy (SEM) analysis. The interaction of these compounds with ctDNA, as their possible mode of action, was studied using multi-spectroscopic techniques and molecular docking. The data suggested that compound **8m** intercalate in the minor groove of DNA.

Keywords: Isoxazole-1,2,3-triazole, Antibacterial agents, Biofilm inhibition, DNA binding, Cytotoxicity, Anti-bacterial.

1. Introduction

Bacterial infections are posing a serious threat to human health and are the leading cause of chronic diseases worldwide. The situation is becoming worst due to the emergence of resistant and new pathogenic bacterial strains [1]. The tremendous increase has been observed in bacterial resistance due to the greater access to antibiotic drugs in developing countries. According to a recent review on antimicrobial resistance; annual mortality associated with antimicrobial resistance (AMR) is approximately 700,000 [2]. Inaction in containing this menace is likely to cause more than 10 million deaths every year by 2050, which accounts for more deaths than that caused by cancers and road accidents. Most of these deaths are expected in developing countries of Asia and Africa [3]. The severity of the global health crisis has propelled the Infectious Disease Society of America (IDSA) to issue the challenge of developing ten new antibiotics by 2020 [4]. Therefore, to confront the global burden of antibacterial resistance, it is necessary to develop new antibiotics which can disrupt the processes necessary for bacterial cell growth and proliferation to fight against bacterial infections.

There are many factors called virulence attributes which help pathogens to survive, multiply and pathogenesis within the host. These factors include adherence, colonisations, and invasive factors, capsule formation, secretion of endotoxins and exotoxins, etc [5]. Instead of the planktonic state, bacterial cells exist in a sessile state within extracellular matrix called a biofilm. The formation of biofilm in pathogens plays an important role in adherence, colonization, defense mechanism and ultimately helps in pathogenesis [6]. Many reports established the direct connection of biofilm formation with bacterial infections such as chronic lung infections, skin infections, periodontitis, endocarditis and nosocomial infections [7-9]. Thus targeting biofilm formation can be helpful to stop the colonization or adhesion of bacterial population at the very initial level and eliminate the infection.

Literature gives strong pieces of evidence regarding heterocyclic scaffolds containing nitrogen and oxygen having potent biological applications [10]. Over the last decades, progress on the pharmacological activity and synthesis of variously substituted triazole/isoxazole derivatives has been added to the scientific literature [11]. Compounds containing a triazole ring have shown a broad spectrum of activities, including anti-inflammatory [12], analgesic [13], antitumor [14], anti-diabetic [15] and anticonvulsive [16]. Additionally, several reports highlight the importance of triazole motif against microbes: bacteria [17], fungi [18], protozoa [19], and viruses [20]. Similarly, isoxazoles are commonly

encountered in a variety of natural products and drugs with a diverse range of pharmacological activities [21]. Isoxazoles have also been previously reported as an antidiabetic, analgesic, antiarrhythmic, anti-inflammatory, antifungal, antibacterial, anticancer, anti-HIV, anti-Alzheimer's disease, etc. [22-23]. Recently, the strategy of generating a new class of azole based antibacterial agents by clubbing together of two or more biologically important azole scaffolds showed the significant potential of inhibiting bacterial growth [24,25]. Some commonly available drugs which contain 1,2,3-triazole and isoxazole unit are shown in Fig. 1. Moreover, reports suggest that the central structural motifs of biological interest, for instance, triazole, when coupled to another heterocyclic ring have manifested therapeutic potential in different domains including against microbial pathogens [26].

Incited by promising results of these scaffolds, herein, we report a series of isoxazole-triazole conjugates and explored their antibacterial potential against two Gram-positive (*Streptococcus pneumoniae* MTCC 655, *Enterococcus faecalis* MTCC 439) and four Gram-negative (*Pseudomonas aeruginosa* ATCC 2453, *Salmonella typhimurium* MTCC 3224, *Klebsiella pneumoniae* ATCC 700603, *Escherichia coli* ATCC 25922) bacterial strains. Toxicity studies using human RBCs and HEK293 (human embryonic kidney cells) confirmed their non-toxic nature, thus supports further pharmacological investigations. To elucidate their mode of action, DNA binding studies were performed using multi-spectroscopic techniques, further supported by molecular docking studies.

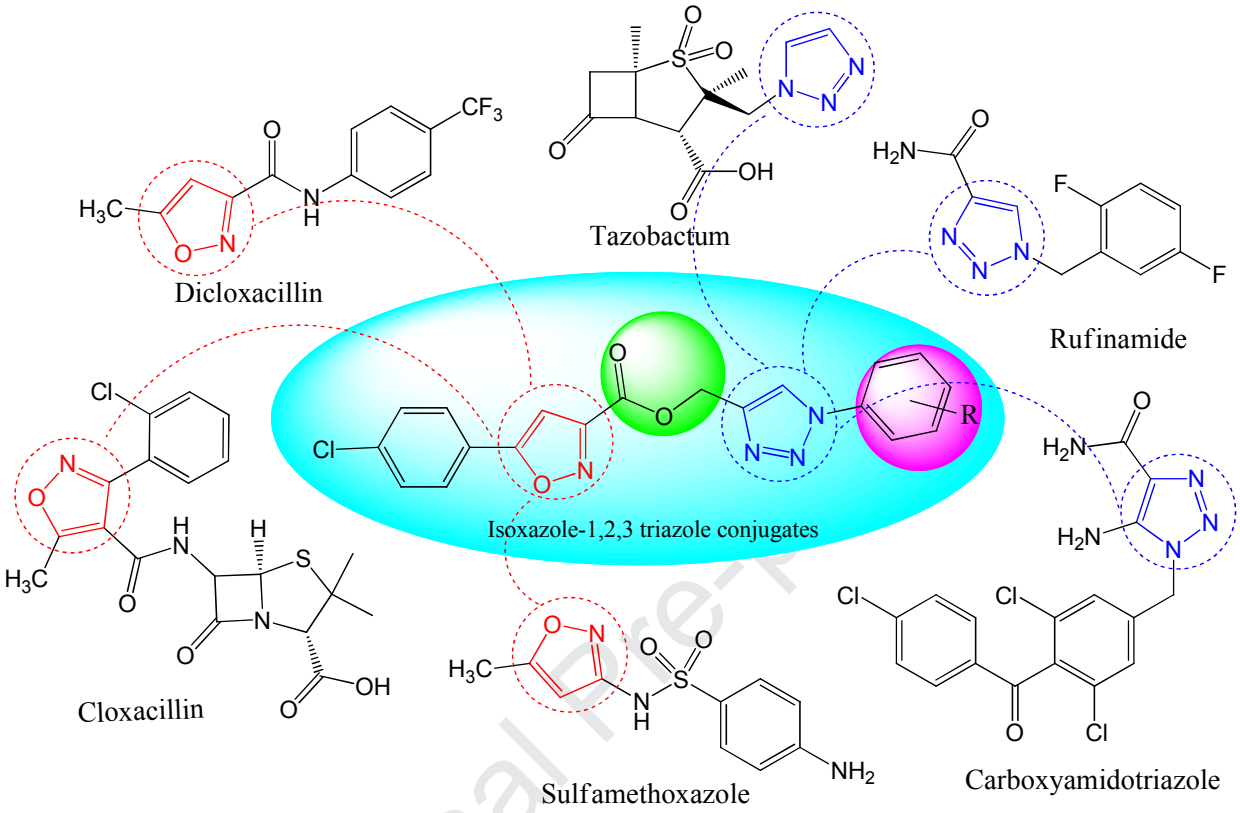

Fig. 1. Rationale design strategy of isoxazole-1,2,3-triazole conjugates. Isoxazole and 1,2,3-triazole moieties of available drugs matched with red and blue dotted lines, respectively. The linker in green sphere joined isoxazole and 1,2,3-triazole moieties. Substituted phenyl group (in pink) is selected for SAR study.

2. Materials and Methods

All the chemicals were purchased from Sigma-Aldrich, USA and used without further purification. Precoated aluminium sheets (Silica gel 60 F_{254}, Merck Germany) were used for thin-layer chromatography (TLC) and spots were visualized under UV light. The IR spectra of compounds were recorded on Agilent Cary 630 FT-IR spectrometer and only major peaks are reported in cm^{-1}. ^{1}H and ^{13}C NMR spectra were obtained at ambient temperature using Bruker Spectrospin DPX-300 MHz, 400 MHz, Agilent 500 MHz FT-NMR in DMSO-*d6* and $CDCl_3$ using tetramethylsilane (TMS) as an internal standard. Splitting patterns designated as follows: s, singlet; d, doublet; t, triplet; m, multiplet. Chemical shift values are given in parts per million (ppm) and coupling constants (*J*) in Hertz (Hz). Mass spectra were recorded on an

Agilent Quadrupole-6150 LC−MS spectrometer. Melting points were recorded on a digital Buchi melting point apparatus (M-560) and were reported uncorrected. Purification of the compounds was done by column chromatography using silica gel (230–400 mesh size) with hexane/ethyl acetate as eluent. Purity was determined by an Agilent RRLC MS 6320 ion trap spectrometer using an XBridge C18 1.7 μm column (50 mm × 2.1 mm). Mobile phase channel A consisted of 5 mM ammonium acetate in water. Mobile phase B consisted of acetonitrile with a flow rate = 0.8 mL/min; detection was done by UV at 214 nm.

2.1. Synthesis of diketoester (3)

As reported earlier [27]. Briefly, in a round bottom flask, sodium metal (22.47 mmol) was dissolved in anhydrous ethanol at 0 ^{o}C to give sodium ethoxide solution. To this freshly prepared solution, a mixture of diethyl oxalate (20 mmol) and *p*-chloroacetophenone (21 mmol) was slowly added. Thick precipitate was formed and reaction mixture was stirred for 3–4 h at room temperature. After completion of the reaction, the precipitate obtained was dissolved in 2 N sulphuric acid (72 ml) and the compound was extracted with diethyl ether, dried over anhydrous Na_2SO_4 and concentrated under reduced pressure and purified using column chromatography.

2.2. Synthesis of isoxazole ethyl ester (4)

As reported earlier [28].Briefly, to the stirred solution of diketo ester **3** (1.0 eq) in anhyd. ethanol was added hydroxylamine hydrochloride (3.0 eq) and the reaction mixture was refluxed for 2½ h. After completion of the reaction, the reaction mixture was cooled to room temperature. The solid precipitate obtained was filtered over the Buckner funnel and washed with cold ethanol. The solid product was dried under *vacuo* to afford isoxazole ethyl ester.

2.3. Synthesis of isoxazole carboxylic acid (5)

As reported earlier [29]. Hydrolysis of isoxazole ethyl ester **4** (1.0 eq) was done by employing freshly prepared LiOH (2M) (4.5 eq.) in THF /H_2O mixture (3:1) for 3 hours to give the corresponding acid in quantitative yield which was used further without purification.

2.4. Synthesis of isoxazole alkyne (6)

In a 50 ml round bottom flask, 5-(3-Chlorophenyl) isoxazole-1-carboxylic acid **5** (4.5 mmol) was dissolved in acetonitrile (10 ml) and cooled to 0 °C followed by slow addition of propargyl alcohol (5.37 mmol). To this solution, NMM (5.37 mmol), HOBt (9.0 mmol) and EDC.HCl (5.4 mmol) were added in small portions. The reaction mixture was brought to

room temperature and the progress of the reaction was checked by TLC. After completion of the reaction, it was concentrated and water was added to the residue. The compound was extracted with ethyl acetate, dried over anhydrous sodium sulphate and concentrated under *vacuo*.

2.4.1. prop-2-yn-1-yl 5-(4-chlorophenyl)isoxazole-3-carboxylate (6)

White solid, mp: 187-189 °C, Yield: 80%, R_f (hexane: ethyl acetate = 7:3): 0.26, IR (neat): ν(cm^{-1}) 3147 (=CH str.), 1734 (C=O str.), 1611 (C=N), 1238 (C-O-N) cm^{-1}. ^{1}H NMR (300 MHz, $CDCl_3$ (*δ* ppm): 8.18 (s, 1H, Ar-*H*), 7.74(d, *J* = 7.2 Hz, 2H, Ar-*H*), 7.55(d, *J* = 6.9 Hz 2H, Ar-*H*), 5.64 (s, 2H, C*H*$_2$), 3.54(s, 1H, ≡C*H*).

2.5. General procedure for the synthesis of azides (7a-q)

To a solution of substituted aniline (3.22 mmol) in ethyl acetate kept at 0 °C was added conc. hydrochloric acid (1.29 mL) followed by drop wise addition of a solution of $NaNO_2$ (3.87 mmol) in water (4.03 mL) over a period of 10 min with constant stirring. After stirring the reaction mixture for 1 h at 0 °C, a solution of NaN_3 (3.87 mmol) in water was added to this mixture and allowed to stir at room temperature for 3 h. After completion of the reaction, the mixture was poured into water, extracted with ethyl acetate, dried over anhyd. sodium sulfate, and concentrated under *vacuo* to give azide, which was used further without purification.

2.6. General procedure for the synthesis of isoxazole-triazole conjugates (8a-q)

To a solution of substituted aryl azide (1.0 mmol) and alkyne (1.0 mmol) in a mixed solvent system, THF/H_2O (1:2, 9mL), were added sodium ascorbate (0.55 mmol) and $CuSO_4 \cdot 5H_2O$ (0.18 mmol). The reaction mixture was stirred overnight at room temperature. After completion of the reaction, the solid obtained was filtered and washed with water. The crude product was purified by silica gel chromatography using ethyl acetate/hexane (3:7) to afford the title compounds.

2.6.1. (1-Phenyl-1*H*-1,2,3-triazol-4-yl)methyl 5-(4-chlorophenyl)isoxazole-3-carboxylate(8a)

Brown solid, mp: 263-265 °C, Yield: 75%, R_f (hexane: ethyl acetate = 7:3): 0.16, IR(neat): ν(cm^{-1}) 3123 (=CH str., triazole, 1746 (C=O str.), 1611 (C=N), 1240 (C-O-N) cm^{-1}, ^{1}H NMR (300 MHz, DMSO-d_6 (*δ* ppm): 8.99 (s, 1H, Ar-*H*), 7.96 (d, *J* = 8.7 Hz, 2H, Ar-*H*), 7.90 (d, *J* = 7.8 Hz, 2H, Ar-*H*), 7.64-7.58 (m, 5H, Ar-*H*), 7.53 (d, *J* = 7.2 Hz, 1H, Ar-*H*), 5.59 (s, 2*H*, C*H*$_2$); ^{13}CNMR (75 MHz, DMSO-d_6) (*δ*, ppm): 170.62, 159.42, 157.12, 142.71, 136.95,

136.25, 130.42, 129.95, 129.37, 128.14, 127.80, 126.10, 125.33, 124.02, 120.73, 101.99, 59.12. LC-MS: *m/z* $[M + H]^+$: 381.10.

2.6.2. 4-(4-(((5-(4-Chlorophenyl)isoxazole-3-carbonyl)oxy)methyl)-1*H*-1,2,3-triazol-1-yl)benzoic acid(8b)

Yellow solid, mp: 261-263 °C, Yield: 77%, R_f. (hexane: ethyl acetate = 7:3): 0.18, IR (neat): ν(cm^{-1}) 3121 (=CH str., triazole, 1741 (C=O str.), 1609 (C=N), 1240 (C-O-N) cm^{-1}.^{1}H NMR (300 MHz, DMSO-d_6). (*δ*, ppm): 13.17 (s, 1H,COO*H*), 9.09 (s, 1H,Ar-*H*), 8.11 (brs, 5H, Ar-*H*), 7.98 (d, *J* = 8.1 Hz, 2H, Ar-*H*), 7.62 (d, *J* = 8.4 Hz, 2H, Ar-*H*), 7.23 (s, 1H, Ar-*H*), 5.61 (s, 2H, CH_2); ^{13}C NMR (75 MHz, DMSO-d_6) (*δ*, ppm): 170.60, 159.38, 157.07, 144.38, 143.06, 139.82, 136.23, 131.94, 129.91, 128.11, 125.29, 124.09, 120.62, 119.74, 101.95, 59.02 LC-MS: *m/z* $[M - H]^+$: 423.11.

2.6.3. (1-(4-methylphenyl)-1H-1,2,3-triazol-4-yl)methyl 5-(4-chlorophenyl)isoxazole-3-carboxylate(8c)

White solid, mp.: 209-211 °C, Yield: 77%, R_f (hexane: ethyl acetate = 7:3) : 0.321, IR (neat): ν(cm^{-1}) 3140 (=CH str., triazole, 1730 (C=O str.), 1613 (C=N), 1233 (C-O-N) cm^{-1}.^{1}H NMR (300 MHz, $CDCl_3$ (*δ*, ppm): 8.06 (s, H, *Ar-H*), 7.66 (d, *J*= 8.4 Hz, 2H, *Ar-H*), 7.54 (d, *J*= 8.4 Hz, 2H, *Ar-H*), 7.39 (d, *J* = 8.7 Hz, 2H, *Ar-H*), 7.25 (d, *J* = 8.1 Hz, 2H, *Ar-H*), 6.86 (s, 1H,*Ar-H*), 5.56 (s, 2H, CH_2), 2.36 (s, 3H, CH_3); ^{13}C NMR (75 MHz, DMSO-d_6) (*δ*, ppm): 170.60, 159.40, 157.11, 142.57, 138.99, 136.24, 135.62, 134.71, 130.72, 129.93, 128.13, 127.79, 126.10, 125.32, 123.85, 120.57, 101.96, 59.11, 21.04. LC-MS: *m/z* $[M + H]^+$: 395.07.

2.6.4. (1-(4-methoxyphenyl)-1*H*-1,2,3-triazol-4-yl)methyl 5-(4-chlorophenyl)isoxazole-3-carboxylate(8d)

Cream solid, mp: 180-182 °C, Yield: 86%, R_f(hexane: ethyl acetate = 7:3): 0.37, IR (neat): ν(cm^{-1}) 3138 (=CH str., triazole, 1730 (C=O str.), 1611 (C=N), 1248 (C-O-N) cm^{-1}.^{1}H NMR (300 MHz, $CDCl_3$) (*δ*, ppm): 8.01 (s, 1H, Ar-*H*), 7.66 (d, *J* = 8.4 Hz, 3H, *Ar-H*), 7.51 (d, *J* = 9 Hz, 2H, *Ar-H*), 7.39(d, *J* = 8.4 Hz, 2H, Ar-*H*), 6.95(d, *J* = 9.0 Hz, 2H, *Ar-H*), 5.55 (s, 2H, CH_2), 3.80(s, 3H, OCH_3); ^{13}CNMR (75 MHz, DMSO-d_6) (*δ*, ppm): 170.60, 159.87, 159.41, 157.11, 142.43, 136.23, 130.33, 129.93, 128.13, 125.31, 123.96, 122.37, 115.37, 101.97, 59.14, 56.04. LC-MS: *m/z* $[M + H]^+$: 411.19.

2.6.5 (1-(4-Fluorophenyl)-1*H*-1,2,3-triazol-4-yl)methyl 5-(4-chlorophenyl)isoxazole-3-carboxylate(8e)

Light brown solid, mp: 181-183 °C, Yield: 54%, R_f(hexane: ethyl acetate = 7:3): 0.39, IR (neat): ν(cm^{-1}) 3155 (=CH str., triazole, 1737 (C=O str.), 1610 (C=N), 1231 (C-O-N) cm^{-1}.^{1}H NMR (300 MHz, DMSO-d_6). (δ, ppm): 8.96 (s, 1H, Ar-*H*), 7.99(d, *J* = 8.4 Hz, 4H, Ar-*H*), 7.64-7.59 (m, 3H, Ar-*H*), 7.47 (t, *J* = 8.7 Hz, 2H, Ar-*H*), 5.59 (s, 2H, CH_2); ^{13}C NMR (75 MHz, DMSO-d_6) (δ, ppm): 170.60, 163.85, 160.57, 159.39, 157.09, 142.71, 136.23, 133.51, 129.93, 128.12, 125.29, 124.26, 123.16, 123.04, 117.40, 117.09, 101.97, 59.06. LC-MS: *m/z* $[M + H]^+$: 399.18.

2.6.6. (1-(4-chlorophenyl)-1*H*-1,2,3-triazol-4-yl)methyl 5-(4-chlorophenyl)isoxazole-3-carboxylate(8f)

white solid, mp: 204-206 °C Yield: 76%, R_f(hexane: ethyl acetate = 7:3): 0.393 IR (neat): ν(cm^{-1}) 3123 (=CH str., triazole, 1737 (C=O str.), 1603 (C=N), 1236 (C-O-N) cm^{-1}.$^{1.}$. ^{1}H NMR (300 MHz, DMSO-d_6). (δ, ppm): 8.98 (s, 1H, Ar-*H*), 7.99-7.96 (m, 4H, Ar-*H*), 7.69-7.61 (m, 4H, Ar-*H*), 7.55 (s, 1H, Ar-*H*), 5.60 (s, 2H, CH_2); ^{13}C NMR (75 MHz, DMSO-d_6) (δ, ppm): 170.61, 159.39, 157.08, 142.87, 136.24, 135.74, 133.65, 130.36, 129.92, 128.12, 125.30, 124.08, 122.39, 101.95, 59.04. LC-MS: *m/z* $[M + H]^+$: 415.2.

2.6.7. (1-(4-nitrophenyl)-1*H*-1,2,3-triazol-4-yl)methyl 5-(4-chlorophenyl)isoxazole-3-carboxylate(8g)

White solid, mp: 203-204 °C, Yield: 78%, R_f(hexane: ethyl acetate = 7:3): 0.387. IR (neat): ν(cm^{-1}) 3125 (=CH str., triazole, 1734 (C=O str.), 1613 (C=N), 1249 (C-O-N) cm^{-1}.^{1}H NMR (300 MHz, DMSO-d_6). (δ, ppm): 9.18 (s, 1H, Ar-*H*), 8.46 (d, *J* = 9.0 Hz, 2H, Ar-*H*), 8.25 (d, *J* = 9.0 Hz, 2H, Ar-*H*), 7.99 (d, *J* = 8.4 Hz, 2H, Ar-*H*), 7.64-7.58 (m, 3H, Ar-*H*), 5.62 (s, 2H, CH_2); ^{13}C NMR (75 MHz, DMSO-d_6) (δ, ppm): 170.61, 162.25, 159.39, 157.06, 147.45, 143.38, 136.29, 133.61, 129.96, 128.15, 126.06, 124.46, 121.32, 101.96, 58.93. LC-MS: *m/z* $[M + H]^+$: 408.0.

2.6.8 (1-(2-chlorophenyl)-1*H*-1,2,3-triazol-4-yl)methyl 5-(4-chlorophenyl)isoxazole-3-carboxylate(8h)

Light brown solid, mp: 127-129 °C, Yield: 81%, R_f(hexane: ethyl acetate = 7:3): 0.472, IR (neat): ν(cm^{-1}) 3162 (=CH str., triazole, 1754 (C=O str.), 1609 (C=N), 1249 (C-O-N) cm^{-1}.^{1}H NMR (300 MHz, DMSO-d_6). (δ, ppm): 8.76 (s, 1H, Ar-*H*), 7.99(d, *J* = 8.4 Hz, 2H, Ar-*H*), 7.79(d, *J* = 7.5 Hz, 2H, Ar-*H*), 7.73(d, *J* = 7.8 Hz, 2H, Ar-*H*), 7.64-7.57 (m, 5H, Ar-*H*), 5.62 (s, 2H, CH_2); ^{13}C NMR (75 MHz, DMSO-d_6) (δ, ppm): 170.62, 159.42, 157.09, 141.69,

136.24, 134.79, 132.26, 131.04, 129.91, 128.96, 128.90, 128.13, 127.87, 125.30, 101.95, 59.0; LC-MS: *m/z* $[M + H]^+$: 414.9.

2.6.9 (1-(2-Nitrophenyl)-1*H*-1,2,3-triazol-4-yl)methyl 5-(4-chlorophenyl)isoxazole-3-carboxylate(8i)

Brown solid, mp: 151-153 °C, Yield: 87%, R_f(hexane: ethyl acetate = 7:3): 0.147, IR (neat): ν(cm^{-1}) 3130 (=CH str., triazole, 1726 (C=O str.), 1611 (C=N), 1238 (C-O-N) cm^{-1}.. ^{1}H NMR (300 MHz, DMSO-d_6). (δ, ppm): 8.89 (s, 1H, Ar-*H*), 8.25 (d, *J* = 7.8 Hz, 1H, Ar-*H*), 8.01-7.84 (m, 5H, Ar-*H*), 7.63 (d, *J* = 9.6 Hz, 3H, Ar-*H*), 5.62 (s, 2H, CH_2); ^{13}C NMR (75 MHz, DMSO-d_6) (δ, ppm): 170.65, 159.40, 157.08, 144.49, 142.36, 136.26, 134.94, 131.84, 129.94, 129.43, 128.15, 127.09, 126.05, 125.31, 101.95, 58.91. LC-MS: *m/z* $[M + H]^+$: 426.07

2.6.10. (1-(2-Fluorophenyl)-1*H*-1,2,3-triazol-4-yl)methyl 5-(4-chlorophenyl)isoxazole-3-carboxylate(8j)

Light brown solid, mp: 150-152 °C, Yield: 68%, R_f(hexane: ethyl acetate = 7:3): 0.454 IR (neat): ν(cm^{-1}) 3173 (=CH str., triazole, 1730 (C=O str.), 1611 (C=N), 1229 (C-O-N) cm^{-1}.. ^{1}H NMR (300 MHz, DMSO-d_6). (δ, ppm): 8.80 (s, 1H, Ar-*H*), 8.00-7.97 (m, 2H, Ar-*H*), 7.89-7.85 (m, 1H, Ar-*H*), 7.63-7.59 (m, 5H, Ar-*H*), 7.48-7.44 (m, 1H, Ar-*H*), 5.61 (s, 2H, CH_2); ^{13}C NMR (75 MHz, DMSO-d_6) (δ, ppm): 170.61, 159.41, 157.08, 155.98, 152.66, 142.19, 136.23, 132.00, 131.00, 129.11, 128.12, 127.31, 127.25, 126.48, 125.29, 125.12, 117.75, 101.93, 58.96. LC-MS: *m/z* $[M + H]^+$: 399.17

2.6.11. (1-(2-Methylphenyl)-1*H*-1,2,3-triazol-4-yl)methyl 5-(4-chlorophenyl)isoxazole-3-carboxylate(8k)

Creamish solid, mp: 153-155 °C, yield: 76%, R_f(hexane: ethyl acetate = 7:3): 0.516, IR (neat): ν(cm^{-1}) 3153 (=CH str., triazole, 1732 (C=O str.), 1611 (C=N), 1251 (C-O-N) cm^{-1}.. ^{1}H NMR (300 MHz, DMSO-d_6). (δ, ppm): 8.66 (s, 1H, Ar-*H*), 7.98 (d, *J* = 8.7 Hz, 2H, Ar-*H*), 7.64-7.59 (m, 3H, Ar-*H*), 7.49-7.45 (m, 4H, Ar-*H*), 5.60(s, 2H, CH_2), 2.17 (s, 3H, CH_3); ^{13}C NMR (75 MHz, DMSO-d_6) (δ, ppm): 170.59, 159.43, 157.12, 141.66, 136.54, 136.23, 133.52, 131.86, 130.41, 129.92, 128.11, 127.49, 127.26, 126.50, 125.29, 101.95, 59.12, 17.88. LC-MS: *m/z* $[M + H]^+$: 395.14.

2.6.12. (1-(2-Methoxyphenyl)-1*H*-1,2,3-triazol-4-yl)methyl 5-(4-chlorophenyl)isoxazole-3-carboxylate(8l)

Cream solid, mp: 138-140 °C, Yield: 83%, R_f(hexane: ethyl acetate = 7:3): 0.356. IR (neat): ν(cm^{-1}) 3140 (=CH str., triazole, 1737 (C=O str.), 1611 (C=N), 1244 (C-O-N) cm^{-1}.. ^{1}H NMR (300 MHz, DMSO-d_6). (δ, ppm): 8.64 (s, 1H, Ar-*H*), 7.99(d, *J* = 8.7 Hz, 2H, Ar-*H*), 7.66-7.59 (m, 4H, Ar-*H*), 7.55 (t, *J* = 7.8 Hz, 1H, Ar-*H*), 7.34(d, *J* = 8.4 Hz, 1H, Ar-*H*), 7.16(t, *J* = 7.5 Hz, 1H, Ar-*H*), 5.59 (s, 2H, CH_2), 3.87 (s, 3H, OCH_3); ^{13}C NMR (75 MHz, DMSO-d_6) (δ, ppm): 170.61, 159.45, 157.13, 141.34, 136.23, 131.38, 129.92, 128.14, 127.70, 126.28, 125.97, 125.32, 12137, 113.52, 101.94, 59.14, 56.62. LC-MS: *m/z*: $[M + H]^+$: 330.1.

2.6.13. (1-(3-Chlorophenyl)-1*H*-1,2,3-triazol-4-yl)methyl 5-(4-chlorophenyl)isoxazole-3-carboxylate(8m)

Off-white solid, mp: 167-169 °C, Yield: 73%, R_f(hexane: ethyl acetate = 7:3): 0.548,. IR (neat): ν(cm^{-1}) 3137 (=CH str., triazole, 1721 (C=O str.), 1611 (C=N), 1250 (C-O-N) cm^{-1}.. ^{1}H NMR (300 MHz, DMSO-d_6). (δ, ppm): 8.74 (s, 1H, Ar-*H*), 7.98 (d, *J* = 8.7 Hz, 2H, Ar-*H*), 7.79-7.58 (m, 7H, Ar-*H*), 5.62 (s, 2H, CH_2); ^{13}C NMR (75 MHz, DMSO-d_6) (δ, ppm): 170.62, 159.42, 157.08, 141.70, 136.24, 134.78, 132.27, 131.05, 129.92, 128.98, 128.89, 128.13, 127.87, 125.28, 101.93, 59.00. LC-MS: m/z: $[M + H]^+$: 368.29.

2.6.14. (1-(3-fluorophenyl)-1H-1,2,3-triazol-4-yl)methyl 5-(4-chlorophenyl)isoxazole-3-carboxylate(8n)

Cream solid, mp: 163-164 °C, Yield: 82%, R_f(hexane: ethyl acetate = 7:3): 0.515. IR (neat): ν(cm^{-1}) 3127 (=CH str., triazole, 1743 (C=O str.), 1612 (C=N), 1238 (C-O-N) cm^{-1}.^{1}H NMR (300 MHz, DMSO-d_6). (δ, ppm): 9.05(s, 1H, Ar-H), 7.99 (d, J = 8.4 Hz, 2H, Ar-*H*), 7.91.-7.82 (m, 2H, Ar-*H*), 7.71-7.61 (m, 4H, Ar-*H*), 7.38 (dt, *J* = 1.8, 8.4 Hz, 1H, Ar-*H*), 5.59 (s, 2H, CH_2); ^{13}C NMR (75 MHz, DMSO-d_6) (δ, ppm): 170.62, 164.49, 159.38, 157.08, 142.88, 138.04, 136.25, 132.46, 132.34, 129.96, 128.14, 125.28, 124.19, 116.65, 108.39, 101.97. LC-MS: *m/z* $[M + H]^+$: 399.4.

2.6.15. (1-(3-methylphenyl)-1*H*-1,2,3-triazol-4-yl)methyl 5-(4-chlorophenyl)isoxazole-3-carboxylate(8o)

Cream solid, mp: 154-156 °C, Yield: 76%, R_f(hexane: ethyl acetate = 7:3): 0.575 , IR (neat): ν(cm^{-1}) 3133 (=CH str., triazole, 1732 (C=O str.), 1612 (C=N), 1237 (C-O-N) cm^{-1}.^{1}H NMR (300 MHz, DMSO-d_6). (δ, ppm): 8.95 (s, 1H, Ar-*H*), 7.97(d, *J* = 6.9 Hz, 2H, Ar-*H*),), 7.56-7.69 (m, 2H, Ar-*H*), 7.62-7.57 (m, 3H, Ar-*H*), 7.48 (t, *J* = 7.8 Hz, 1H, Ar-*H*), 7.31 (d, *J* = 7.5 Hz, 1H, Ar-*H*), 5.59 (s, 2H, CH_2), 2.41 (s, 3H, CH_3); ^{13}C NMR (75 MHz, DMSO-d_6) (δ,

ppm): 170.59, 159.40, 157.09, 142.62, 140.16, 136.89, 136.23, 130.16, 129.91, 128.10, 125.29, 123.89, 123.53, 121.09, 117.76, 101.92, 59.11, 21.34. LC-MS: *m/z* $[M + H]^+$: 395.0

2.6.16. (1-(3-methoxyphenyl)-1H-1,2,3-triazol-4-yl)methyl 5-(4-chlorophenyl)isoxazole-3-carboxylate(8p)

Pink solid, mp: 150-152 °C, Yield: 78%, R_f(hexane: ethyl acetate = 7:3): 0.516, IR (neat): ν(cm^{-1}) 3142 (=CH str., triazole, 1730 (C=O str.), 1613 (C=N), 1231 (C-O-N) cm^{-1}. ^{1}H NMR (300 MHz, DMSO-d_6). (δ, ppm): 8.99 (s, 1H, Ar-*H*), 7.99 (d, *J* = 7.2 Hz, 2H, Ar-*H*), 7.63 (d, *J* = 7.2 Hz, 3H, Ar-*H*), 7.58-7.51 (m, 3H, Ar-*H*), 7.09-7.07 (m, 1H, Ar-*H*), 5.59 (s, 1H, CH_2), 3.87 (s, 3H, OCH_3), ^{13}C NMR (75 MHz, DMSO-d_6) (δ, ppm): 170.62, 160.67, 159.39, 157.11 142.64, 137.97, 136.25, 131.37, 129.95, 128.15, 125.31, 124.12, 115.12, 112.67, 106.31, 101.96, 59.8, 56.11. LC-MS: *m/z* $[M + H]^+$: 410.8.

2.6.17. (1-(3-Nitrophenyl)-1*H*-1,2,3-triazol-4-yl)methyl 5-(4-chlorophenyl)isoxazole-3-carboxylate(8q) Dark brown solid, mp: 160-162 °C, Yield: 87%, R_f(hexane: ethyl acetate = 7:3): 0.375, IR (neat): ν(cm^{-1}) 3155 (=CH str., triazole, 1739 (C=O str.), 1611 (C=N), 1235 (C-O-N) cm^{-1}.^{1}H NMR (300 MHz, DMSO-d_6). (δ, ppm): 9.23 (s, 1H, Ar-*H*), 8.76 (s, 1H, Ar-*H*), 8.44 (d, *J* = 8.1 Hz, 1H, Ar-*H*), 8.35 (d, *J* = 8.1 Hz, 1H, Ar-*H*), 7.99 (d, *J* = 8.7 Hz, 2H, Ar-*H*), 7.92 (t, *J* = 8.1 Hz, 1H, Ar-*H*), 7.65-7.61 (m, 2H, Ar-*H*), 5.62 (s, 2H, CH_2); ^{13}C NMR (75 MHz, DMSO-d_6) (δ, ppm): 170.61, 159.38, 157.06, 148.98, 143.17, 137.49, 136.24, 132.03, 129.91, 128.10, 126.71, 125.28, 124.47, 123.77, 115.42, 101.93, 58.96. LC-MS: *m/z*: $[M + H]^+$:380.2.

2.7. *In vitro* antimicrobial activity

All the compounds (**8a-8q)** were screened for their *in vitro* antibacterial activity against two Gram-positive (*S. pneumoniae, E. faecalis*) and four Gram-negative strains (*P. aeruginosa, S. typhimurium, K. pneumoniae, E. coli*) bacterialstrains using broth dilution assay according to the standard protocol for antibacterial assessment by NCCLS. Ciprofloxacin (CIP) was used as positive control for the study. The compounds were dissolved in DMSO and serially diluted in nutrient broth medium to achieve the final concentration of DMSO less than 4%. Varying concentrations (1000 to 7.8 µg/mL) of compounds were dispensed into a 96-well plate in nutrient broth medium in a final volume of 100 µL. Then, 100 µL of bacterial cells (approximate 2.5×10^5 cells/mL) were dispensed into each well of 96-well plate (Tarson) and incubated at 37 °C for 24 h. After incubation period each well was analyzed for the presence or absence of visual growth of bacterial cells. The

lowest concentration of the test compound at which no visible growth occurs represents its MIC value. Moreover, after incubation, the growth was measured turbidometrically at 585 nm using a Thermo MultiskanGo spectrophotometer. The IC_{50} value was defined as the concentration of the test compound that causes 50% decrease in absorbance compared with that of the control (no test compound). Log_{10} concentration versus % growth inhibition scattered graph was plotted to calculate the IC_{50} values of the test compounds.

2.8. Growth curve studies

The bacterial cells were freshly revived by subculture on the nutrient agar plate. A loopful of inoculums was introduced into the nutrient broth and cells were grown for 16 h at 37 °C before use. Approximately 2×10^5 cells/mL was then inoculated into the freshly prepared 50 mL sterile nutrient broth medium. Different concentrations, equivalent to 2MIC (250 µg/mL), MIC (125 µg/mL), MIC/2 (62.5 µg/mL), of compounds were added separately into the conical flasks containing inoculated medium and incubated at 37 °C and 160 rpm. 7.5 µg/mL concentration of CIP was used as positive control. At predetermined time periods (0, 2, 4, 6, 8, 10, 12, 14, 16, 18, 20, 22, and 24 after incubation with agitation at 37 °C), 1 mL aliquot to each sample was removed from the conical flask and growth was measured turbidometrically at 585 nm using Thermo Multiskan spectrophotometer. Optical density was recorded for each concentration against time (h).

2.9. *In vitro* cytotoxicity

HEK293 cells were cultured and maintained as a monolayer in Dulbecco's Modified Eagle's Medium (DMEM, Sigma) supplemented with 10% fetal calf serum (Gibco-life technologies, Thermo Fisher Scientific (USA) and antibiotics (100 IU ml^{-1} of penicillin and 100 mg mL^{-1} of streptomycin, Sigma). The cells were cultured at 37 °C in a humidified atmosphere and 5% CO_2. Exponentially growing cells were plated at 1.2×10^4 cells per well into 96-well plates and incubated for 48 h before the addition of the compounds/metronidazole. Stock solutions of compounds were initially dissolved in 20% (v/v) DMSO and further diluted with fresh complete medium. The growth-inhibitory effects of the compounds were measured using standard tetrazolium MTT assay. After 48 h of incubation at 37 °C, the medium was removed and 25 µL of MTT (5 mg ml^{-1}) in 100 µL of serum free medium was added to each well. The plates were incubated at 37 °C for 4 h. At the end of the incubation period, the medium was removed and 100 µL DMSO was added to each well. The metabolized MTT product was dissolved in DMSO and quantified by reading

the absorbance at 570 nm using an ELISA plate reader. All assays were performed in triplicate. Percent viability was defined as the relative absorbance of treated versus untreated control cells.

2.10. Biofilm inhibition assay

Biofilm formation in *E. coli* and *S. pneumoniae* was determined by semi-quantitative method using XTT (2,3-bis(2-methoxy-4-nitro-5-sulphophenyl)-5-[(phenylamino) carbonyl]-2H-tetrazolium-hydroxide) reduction assay with slight modification in previously known method [30]. Briefly, aliquots of 100 µL of standardized cell suspension test organisms prepared in sterile nutrient broth medium containing 0.5% additional glucose and poured into the wells of micro-titre plate. The plate was incubated at 37 °C for 24 h in static condition to establish biofilm. After incubation period, the medium was discarded and the plate was gently washed with PBS to remove non-adherent cells. Further, 100 µL of freshly prepared medium containing various concentrations of compound **8m** was added to the wells. The plate was again incubated at 37 °C for 24 h under static condition to determine the metabolic activity of biofilm. The medium was discarded and washed with PBS to remove the non-adherent cells followed by the addition of 100 µL of prepared XTT salt solution (HiMedia, India). The plate was incubated at 37 °C in dark for 90 min. Bacterial dehydrogenase activity reduces XTT tetrazolium salt to XTT formazan, resulting in colorimetric change (turns to orange) that was correlated with cell viability. The colorimetric changes were measured spectrophotometrically at 490 nm. The % inhibition data were interpreted from dose-response curves.

2.11. Biofilm formation assessment by SEM analysis

Biofilm inhibition property of compound **8m** was also determined by scanning electron microscopy (SEM) in *E. coli*. The sophisticated analytical instrumentation facility (SAIF) of All India Institute of Medical Sciences, New Delhi was availed for instrumentation support. 3 mL of sterile nutrient broth containing 0.5% additional glucose was poured into the 6 well plate (Tarson) and incubated with freshly prepared primary culture of *E. coli*. 10 mm^2 of glass pieces were sterilized and dispensed into the medium for biofilm formation on the surface. The plate was incubated at 37 °C for 24 h. After incubation, the glass pieces were gently washed with sterile PBS and aseptically transferred into fresh medium followed by addition of test compound at 250 µg/mL and 500 µg/mL concentrations. The plate was then incubated at 37 °C for next 24 h. After incubation, the glass pieces was removed and gently

washed with PBS and kept in fixative (2.5% glutaraldehyde and 2% paraformaldehyde in 0.1 M phosphate buffer, pH 7.4) overnight. Samples were again washed with PBS and dried to examine under scanning electron microscope.

2.12. DNA binding studies

ctDNA was purchased from Sigma Aldrich (St. Louis, USA) and was used without further purification. The solutions were prepared in tris-HCl buffer (pH 7.2). The concentration of ctDNA was determined from absorption spectroscopy by using the average extinction coefficient value of 6600 $M^{-1}cm^{-1}$ of a single nucleotide at 260 nm, which was further validated by Nano Drop. The purity of DNA solution was checked by taking absorbance ratio A_{260nm}/A_{280nm} [31].

2.12.1. UV-Vis spectroscopy

Absorption spectra were recorded on Analytik Jena Specord-250 spectrophotometer (Konrad-Zuse-Strasse Jena, Germany). Quartz cuvettes of 1.0 cm were used. Absorbance titrations were performed by maintaining fixed concentration of **8m** (5 μM) and varying the concentrations of ctDNA (0-60 μM) [32].

2.12.2. Steady state fluorescence

Fluorescence emission spectra were recorded using a Cary Eclipse spectrofluorometer (Varian, USA) equipped with a 150 W xenon lamp in a 1.0 cm quartz cell (Santa Clara, CA) and a thermostated water bath, in an emission wavelength range of 450-600 nm upon excitation at 420 nm. Fluorescence spectra were acquired by maintaining the concentration **8m** constant (5 μM) and varying the concentrations of ctDNA (0-80 μM) at 298K [33].

2.12.3. CD Spectroscopy

Jasco-715 spectropolarimeter, equipped with a microcomputer, and 1.0 cm quartz cell was used to record the CD spectra. All the CD measurements were carried out at 298K using a thermostatically controlled cell holder attached to a Neslab RTE-110 water bath with an accuracy of ±0.1 K. All the CD spectra were recorded in the range of 200-350 nm at a scan speed of 50 nm/min [34].

2.13. Docking studies

Docking of compound **8m** with the DNA dodecamer duplex of sequence d(CpGpCpGpApApTpTpCpGpCpG) (PDB ID: 8BNA) was performed using AutoDock Vina 4.2. The structure of compound **8m** was drawn using ChemDraw and converted into PDB

format using online free web server of National Cancer Institute (NCI) named SMILES translator tool (http://cactus.nci.nih.gov/translate/). The desired format of docking *i.e.* PDBQT was obtained using ADL tools. The complete DNA dodecamer was covered within grid box and used for docking process. The interactions between compound **8m** and DNA was visualized by using Pymol [35]. The validity of the docking protocol adopted in this study was performed by re-docking the ligand (HOECHST-33258) present in the X-ray crystal structure of DNA (PDB ID: 8BNA) and comparing the RMSD between the docked and crystal structure poses as described previously [36]. The binding affinity of ligands towards DNA was estimated using the following relation, as described earlier [37].

$$\Delta G = -RT \ln K_a$$

where, *R* and *T* are the universal gas constant (=1.987 cal/mol/K), and temperature (=298K) respectively

3. Results and discussion

3.1. Chemistry

A series of novel isoxazole-1,2,3-triazole conjugates (**8a-q**) was synthesized as shown in Scheme 1. Commercially available *p*-chloroacetophenone (**1**) and diethyl oxalate (**2**) were converted into diketoester (**3**) *via* oxalylation process in the presence of freshly prepared sodium ethoxide. Further, the diketoester (**3**) on reaction with hydroxylamine hydrochloride in absolute ethanol at reflux condition underwent [3+2] cyclo-condensation reaction to give isoxazole ethyl ester (**4**). Basic hydrolysis of isoxazole ethyl ester by employing freshly prepared LiOH (2M) in THF/H_2O mixture for 2½ h gave the corresponding acid in quantitative yield. Further 5-(4-chlorophenyl) isoxazole-3-carboxylic acid (**5**) was propargylated in the presence of hydroxyl benzotriazole (HOBt) and 1-(3-dimethylaminopropyl)-3 ethylcarbodiimide (EDC.HCl) in acetonitrile to yield corresponding alkyne (**6**). All the intermediates were purified by column chromatography to give desired compounds in moderate to high yields as confirmed by spectroscopic analysis. In another set of reaction, variously substituted aniline containing either electron-withdrawing or electron-donating groups were converted into their corresponding azides (**7a-q**) *via* diazotization using sodium nitrite and hydrochloric acid followed by sodium azide treatment. Finally, azide and alkyne underwent Cu(I)-catalyzed [3+2] cycloaddition reaction in the presence of a catalytic amount of $CuSO_4$ and sodium ascorbate (NaAsc) in THF/H_2O (1:2) mixture to yield the title compounds (**8a-q)** in good to excellent yield (Scheme 1). The proposed structures were

confirmed by elemental analysis, FT-IR, ^{1}H, ^{13}C NMR & Mass spectral data, and purity was checked by an Agilent RRLC MS 6320 ion trap spectrometer.

In the IR spectra of all the compounds (**8a-q**), the main evidence for their formation came from the disappearance of absorption band at 2090 cm^{-1} corresponding to azide functionality indicating that azide had been completely consumed in the reaction and the peaks corresponding to alkyne ≡CH and C≡C which appeared in the range 3250-3376 cm^{-1} and 2112-2137 cm^{-1} respectively were also absent from their spectra. All the synthesized compounds (**8a-q**) gave the characteristic peak of triazole ring in the region 3065-3189 cm^{-1} as broad absorption band. All the other absorption bands also appeared in the expected regions.

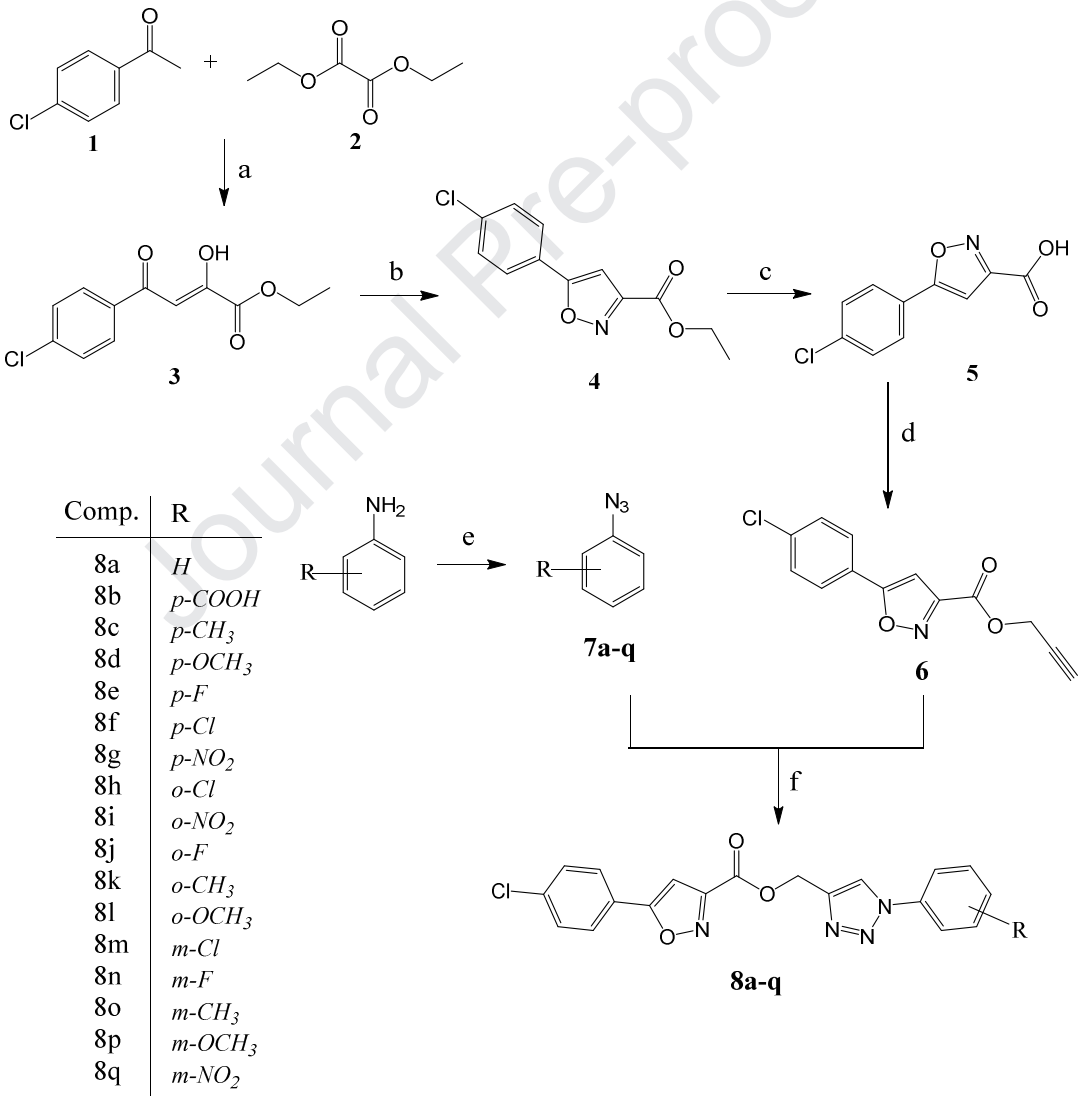

Comp.	R
8a	*H*
8b	*p-COOH*
8c	*p-CH_3*
8d	*p-OCH_3*
8e	*p-F*
8f	*p-Cl*
8g	*p-NO_2*
8h	*o-Cl*
8i	*o-NO_2*
8j	*o-F*
8k	*o-CH_3*
8l	*o-OCH_3*
8m	*m-Cl*
8n	*m-F*
8o	*m-CH_3*
8p	*m-OCH_3*
8q	*m-NO_2*

Scheme 1: Synthesis of Isoxazole-1,2,3-triazole conjugate: Reagents and conditions: (a) Na metal, C_2H_5OH, 4 h, r.t., 70% (b) C_2H_5OH, $NH_2OH.HCl$, 2½ h, 78% (c) THF:H_2O, LiOH,

2½ h, r.t., 95% (d) EDC.HCl, HOBt, acetonitrile, Propargyl alcohol, r.t., 80% (e) $NaNO_2$, HCl, NaN_3, 92-98% (f) $CuSO_4.5H_2O$, NaASc, THF:H_2O, overnight, r.t., 54-87%.

In the ^{1}H NMR spectra, these compounds showed a sharp singlet in the region 7.18-7.67 ppm assigned to triazole ring, confirming its formation. The characteristic singlets at 5.54-4.66 ppm and 5.50-4.36 ppm were also observed for O*CH*$_2$ and C_6H_5*CH*$_2$ protons of triazole derivatives **8a**-**q** respectively. While a sharp singlet corresponding to ≡C*H* group which appeared in the region 2.49-2.57 ppm was absent from the spectra. Besides, all the aromatic and aliphatic protons appeared at their expected chemical shifts and integral values.

The formation of the triazole ring was further confirmed by ^{13}C NMR spectral data in which both the carbons of triazole ring appeared in the range 120.23-127.34 ppm and 138.32-145.92 ppm respectively. The carbon signals of O*C*H_2 and C_6H_5*C*H_2 groups were resonated at 62.16- 65.23 ppm and 54.25-55.99 ppm respectively, while all the other carbons gave peaks at their expected values.

The mass spectra of most of the compounds showed $[M+H]^+$ and $[M-H]^-$ peak which was per their molecular formula thus further confirming their formation. The isoxazole alkyne (6) showed $[M+Na]^+$peak. In the mass spectra of compound **8m**, fragmentation was observed and no peak corresponding to molecular ion peak was observed.

3.2. *In vitro* antimicrobial activity

Antimicrobial screening against two Gram-positive (*S. pneumoniae, E. faecalis*) and four Gram-negative strains (*P. aeruginosa, S. typhimurium, K. pneumoniae, E. coli*) bacterial strains was done using microdilution method [38]. CIP was used as a reference drug and the results are presented as IC_{50} in µg/mL (Table 1). In the preliminary in vitro antibacterial screening, compounds showed selective inhibition of bacterial strains across the screening panel. We synthesized 17 compounds with different substitution on benzene attached to the triazole moiety. Methyl, methoxy, halides *(-Cl* and *-F*), carboxylic and nitro group were substituted at different positions. Although no strong structure-activity relationship could be established, but it was observed based on substitution of various groups at different position of phenyl group, compounds became selective inhibitor against the respective bacterial strain. Compounds **8a-b**, **8d-f**, **8m**, **8o** and **8q** showed good to moderate activity against selective bacterial strains. The Compound **8a** showed moderate activity against *S. pneumoniae and K. pneumoniae* with IC_{50} values of 295.8 and 274.4 µg/mL, respectively. Compound **8b** with *p*-

COOH substitution increased its activity particularly against *P. aeruginosa* with IC_{50} value of 67.6 µg/mL. This compound showed significant inhibition of Gram-negative as well as Gram-positive bacteria. Compound **8d** with *p*-methoxy substitution selectively inhibited *S. typhimurium, S. pneumoniae* and *E. coli* with IC_{50} values of 244.9, 325.1 and 239.8 µg/mL, respectively. Similarly, the substitution of *–F* at para position enabled compounds **8e** as a potent antibacterial agent which selectively inhibited *K. pneumoniae, P. aeruginosa* and *S. pneumoniae* with IC_{50} values of 157.4, 212.3 and 228.0 µg/mL, respectively. Compound **8f** with substitution of *–Cl* at para position showed increased activity against all the bacterial strains. After changing the position of chlorine on meta-position as in compound **8m**, it showed good to moderate activity against all the bacterial strains with IC_{50} values less than 100 µg/mL except *K. pneumonia* (IC_{50} value = 105.9 µg/mL). Moreover, the substitution with *p–COOH* and *–Cl* is responsible for antibacterial activity of compounds which also depicted in Table 1. It showed good activity against Gram-positive bacteria *S. pneumoniae* and *E. faecalis* with potent antibacterial potential having IC_{50} values 74.13 and 44.7 µg/mL, respectively. Thus, based on the above observations, we selected compound **8b** and **8m**, as it showed good to moderate activity against all the strains used in the study, for further biological evaluation.

Table 1. *In vitro* antibacterial activity of compounds (**8a-q**) against Gram-positive and Gram-negative strains in µg/mL.

Compound	IC_{50} in µg/mL					
	P. aeruginosa	*S. typhimurium*	*S. pneumoniae*	*E. faecalis*	*K. pneumoniae*	*E. coli*
8a	544.50	903.64	295.80	482.21	274.78	332.12
8b	67.60	199.06	153.81	114.29	136.77	154.88
8c	676.08	601.17	699.84	812.83	>1000	281.83
8d	950.60	244.90	325.08	519.99	496.59	239.80
8e	212.32	413.23	228.03	790.67	157.39	457.08
8f	153.81	270.39	167.10	171.00	183.23	213.79
8g	948.90	>1000	331.13	>1000	>1000	831.76
8h	448.74	428.54	805.37	>1000	767.36	363.07

8i	628.05	400.49	538.26	788.86	>1000	832.88
8j	397.19	564.93	639.73	383.7	>1000	891.22
8k	322.84	>1000	707.94	>1000	812.83	891.25
8l	110.92	737.90	>1000	578.09	>1000	>1000
8m	92.25	165.19	74.13	44.66	105.92	83.17
8n	948.41	512.86	301.99	201.37	346.73	154.88
8o	197.69	393.55	360.57	542.00	>1000	1095.52
8p	315.50	712.85	634.16	271.64	287.07	524.80
8q	252.34	292.41	194.28	234.42	454.98	776.24

3.3. Cytotoxicity assessment of lead inhibitors by hemolysis and MTT assays

3.3.1. Hemolytic assay

Based on preliminary antibacterial results, compounds **8b** and **8m** were selected to evaluate their cytotoxicity on human red blood cells as well as cell line. The hemolytic assay was performed to check the toxicity of the selected compounds (**8b** and **8m**) on human red blood cells (hRBCs) [39]. At 1 mg/mL concentration, **8b** and **8m** exhibited moderate toxicity causing only 7% and 30% hemolysis, respectively compared to the standard drug CIP with 35% hemolysis. However, at 100 µg/mL concentration these compounds exhibited fairly less toxicity causing only 0.6% and 4% cell lysis, respectively. At 25 µg/mL concentration, these compounds were completely safe causing only 0.05% and 1% cell lysis, respectively (Fig. 2).

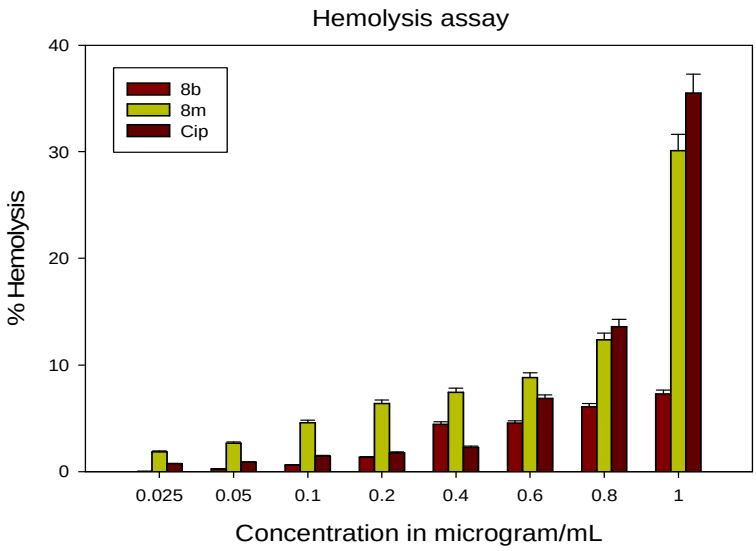

Fig. 2. Hemolysis assay of compounds **8b** and **8m** showing % lysis of human RBCs.

3.3.2. Inhibition of cell proliferation by MTT assay

To evaluate the cytotoxicity effect of selected compounds, human embryonic kidney cells (HEK293) were used. The compounds were screened with the help of a standard MTT assay in the concentration range of 0-200 µM, for 48 h [40]. Interestingly, the results show that the treatment of these compounds doesn't affect the viability of HEK293 cells even at 200 µM concentration. These results suggested that the selected compounds **8b** and **8m** were non-cytotoxic to HEK293 cells in the tested concentration range as shown in Fig. 3. From these cell viability results, we can speculate that these molecules may be taken as promising lead molecules against bacterial infection, as shown in sub-micromolar concentration ranges they do not possess toxicity towards normal embryonic human kidney cells, but for bacterial cells.

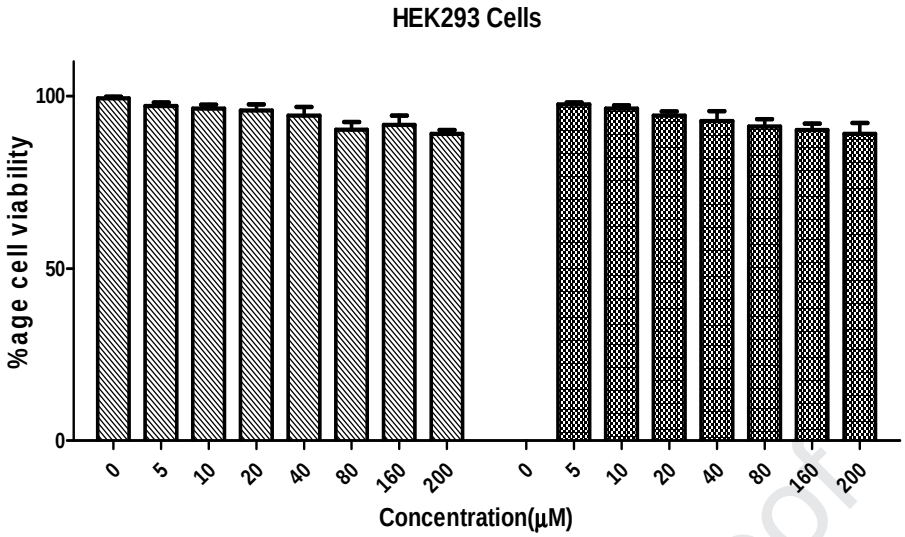

Fig. 3. MTT assay results at concentration range of 0-200 µM of **8b** (left) and; **8m** (right).

3.4. Growth curve

To investigate the effect of lead compounds, growth curve studies were performed against specific susceptible bacterial strains. Compound **8m** was selected as a lead inhibitor to perform further biological studies. We also performed growth curve study for **8b** against *P. aeruginosa*. Growth curve study for compound **8m** was performed against *S. pneumoniae, E. coli* and *E. faecalis* strains. CIP was used as a standard drug while untreated cells were used as positive control. The results showed that significant growth inhibition of *P. aeruginosa* and *S. pneumoniae* occurred due to the presence of compounds **8b** and **8m**, respectively. At higher concentrations *i.e.* 2MIC and MIC of both compounds, an extending lag phase up to 24 h were observed in *P. aeruginosa* as well as *S. pneumoniae* (Fig. 4). Moreover, at low concentration of compound **8b**, the lag phase ended in between 4-6 h in *P. aeruginosa.* Similarly, at the sub-MIC concentration of the compound, the cells of *S. pneumoniae* enter into log phase between 2-4 h. Further, compound **8m** showed moderate growth inhibition against *E. coli* and *E. faecalis* strains. Although, no measurable growth occurred in presence of 2MIC concentration, the cells were grown with very less growth rate at MIC concentration of compound **8m**. There was not any significant change in growth in the presence of sub-MIC concentration against *E. coli* and *E. faecalis.* Thus the above observations indicate the bactericidal nature of compounds **8b** and **8m** against *P. aeruginosa* and *S. pneumoniae,* respectively. Compound **8m** was found more effective towards specific Gram-positive bacterium *S. pneumoniae.*

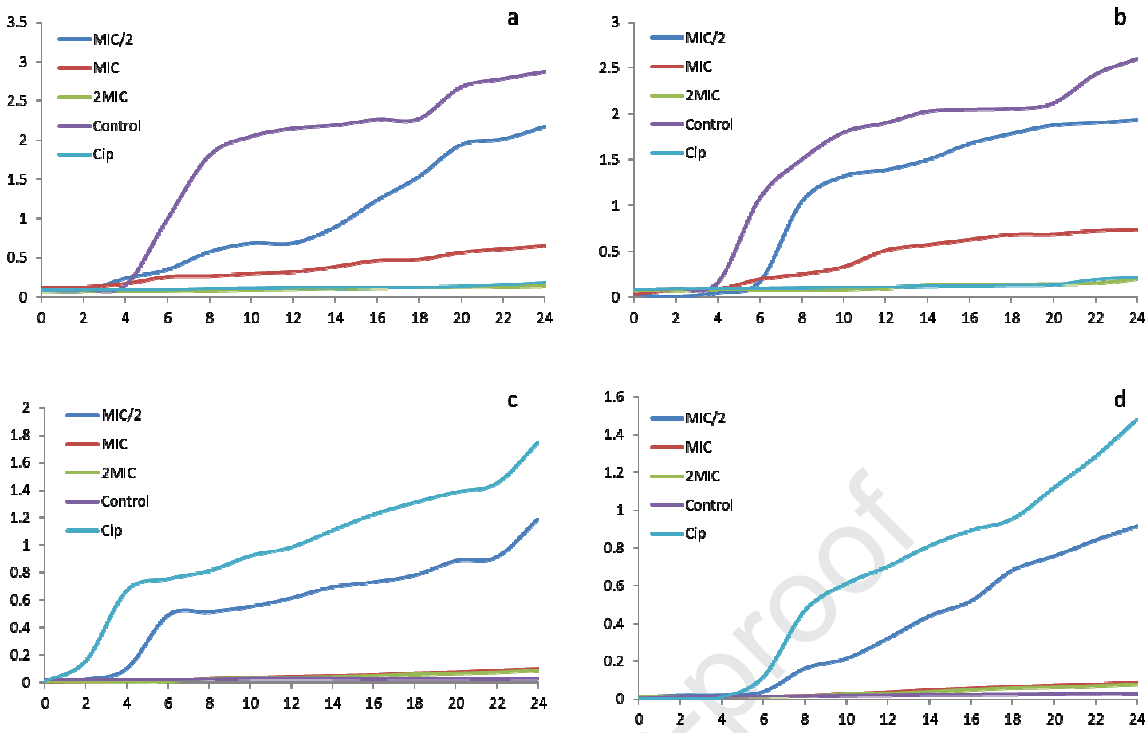

Fig. 4. Dose dependent growth curve of *E. coli* (a); *E. faecalis* (b); *S. pneumoniae* (c) in presence of **8m**; and (d) *P. aeruginosa* in presence of compound **8m**. No growth occurs in the presence of high concentration *i.e.* 2MIC and MIC concentration of compounds **8b** and **8m**.

3.5. Assessment of biofilm formation

On the basis of better antibacterial potential against most of the bacterial strains used in the study as well as toxicity, compound **8m** was selected for further biological assays. The attribute of biofilm formation in pathogenic microorganism plays an important role in virulence. The biofilm inhibition assessment using XTT was performed against *E. coli*, *S. pneumoniae* and *E. faecalis* bacterial strains. The concentrations equal to 8MIC, 4MIC, 2MIC and MIC were used to explore it biofilm inhibition activity. The results indicated that compound **8m** significantly inhibit biofilm formation in *S. pneumoniae* and *E. faecalis* bacterial strains. Although, the effect of compound **8m** against biofilm formation by *E. coli* was comparatively low at lower concentrations it significantly inhibit biofilm formation at 8MIC concentration (Fig. 5).

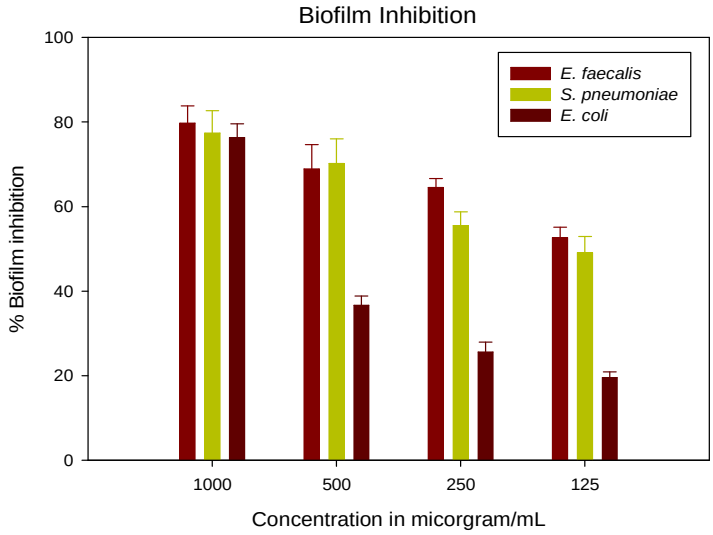

Fig. 5. Biofilm inhibition by XTT assay. Percentage of biofilm inhibition in *E. coli*, *S. pneumoniae* and *E. faecalis* in presence of to 8MIC, 4MIC, 2MIC and MIC concentration of compound **8m.**

The quantitative assessment of biofilm formation by XTT assay was further examined under scanning electron microscopy (SEM). Biofilm formation on the surface of materials occurs due to the secretion of the extracellular matrix which primarily consists of polysaccharide. Two concentrations equal to 4MIC and 2MIC values of compound **8m** were taken to compare the efficacy against biofilm formation with untreated cells. The cells in untreated samples appeared in clusters and embedded in the extracellular matrix (Fig. 6). The sample treated with 4MIC concentration showed very few scattered bacterial cells. Similarly, significant damage in biofilm formation showed at 2MIC concentration (Fig. 6). The results indicated the inhibition of biofilm formation after exposed to compound **8m** and strongly support the data of the previous experiment.

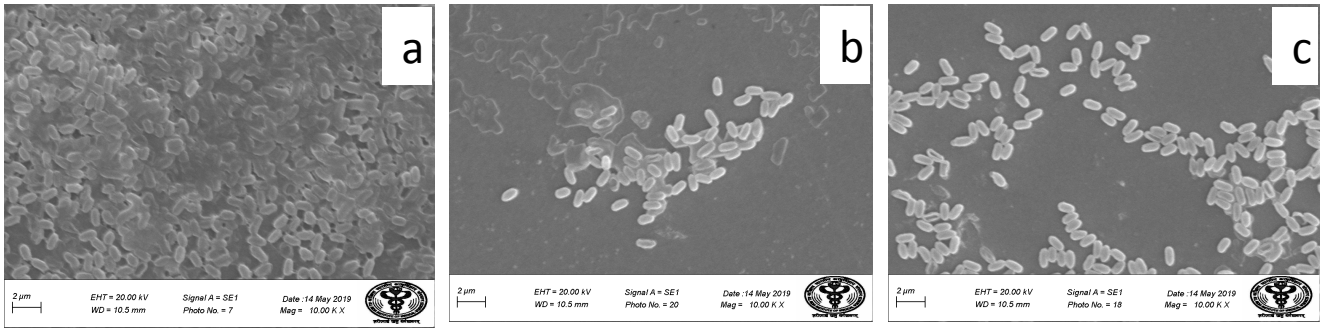

Fig. 6. Scanning electron microscopy of biofilm formation by *E. coli*. in a) untreated sample; b) sample exposed to 4MIC; and c) 2MIC concentration of compound **8m**.

3.6. DNA Binding Studies

The cleavage of DNA due to the binding of some heterocyclic compounds has been explored and reported in the literature [41-43]. Some reports mainly emphasize the efficacy of isoxazole and 1,2,3-triazole containing compounds as potential DNA binding agents which eventually used as antibacterial [44-46]. Thus, we hypothesized DNA as a primary target for our designed compounds. All the experiments of DNA binding studies were performed with compound **8m**.

3.6.1. Electronic/UV-visible absorption spectral studies

UV-Visible spectroscopy is the most widely used technique to detect and identify interactions between small molecules with biomolecules and formation of a complex. The strength of interaction was correlated with the magnitude of change in absorbance or shift in the peak position [47]. The ability of ctDNA to interact with small molecules was evaluated by hypochromism or hyperchromism. The UV absorption spectrum of **8m** with increasing concentrations of ctDNA is shown in Fig. 7. In the absence of DNA, compound **8m** showed maximum absorbance at 420 nm. On addition of first DNA titer (5µM), absorbance is increased indicating DNA-**8m** complex formation. On subsequent additions of DNA, hyperchromism with slight blue shift was observed.

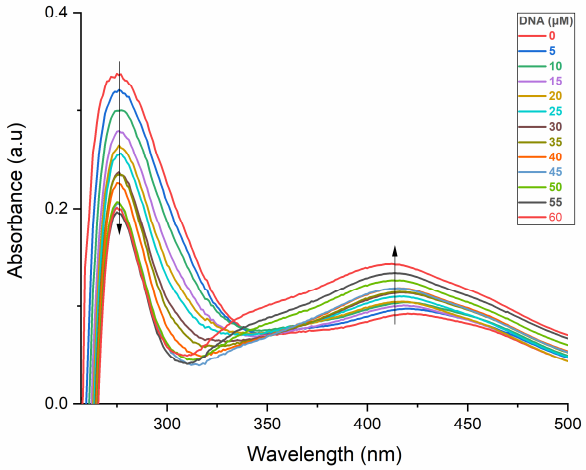

Fig. 7. Absorbance spectra of **8m** with increasing concentrations of ct-DNA (0-60 µM)

3.6.2. Fluorimetric Studies

Because of its high sensitivity, selectivity and convenience, fluorescence emission spectroscopy is widely used to get insights into the binding mode of small molecules with biomolecular structures [48]. Since the endogenous fluorescence property of DNA is poor, fluorescence spectra of compound **8m** were studied with increasing concentrations of ctDNA

at 298K. Fig. 8 shows the fluorescence spectra of **8m** with increasing concentrations of ctDNA (0-80 µM) at 298 K, with emission maxima at 562 nm upon excitation at 420 nm. On subsequent addition of ctDNA, the emission intensity increases significantly without any significant change in emission maxima which is direct evidence for the interaction between **8m** and ctDNA. The absence of quenching effect and the subsequent increase in emission intensity might be attributed to the hydrophobic environment of compound inside the DNA helix as quenching occurs due to photoelectron transfer from the guanine base of DNA to the excited states of the molecule. The emission data demonstrate that **8m** binds with ctDNA through intercalative mode.

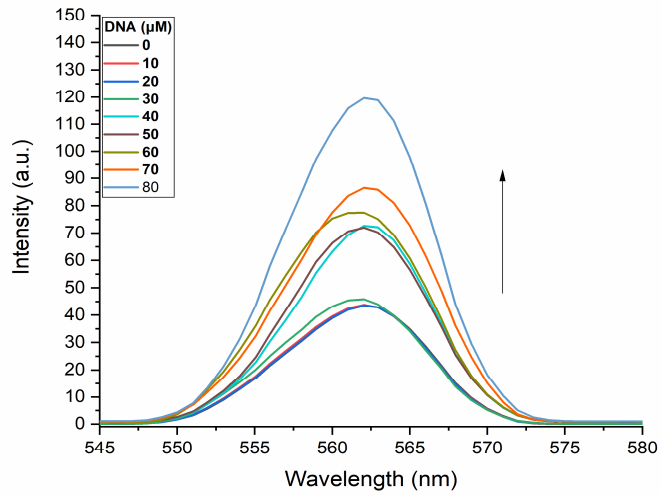

Fig. 8. Fluorescence emission spectra of compound **8m** with increasing concentrations of ctDNA (0-80 µM) at 298K.

3.6.3. Circular dichroism spectroscopy

CD spectroscopy is a highly sensitive technique employed here to investigate the conformational changes in secondary structure and molecular orientations relative to DNA helix. The CD spectrum of ctDNA exhibits a positive band at ~275 nm due to base stacking and a negative band at ~245 nm due to the right-handed helicity of B-DNA form which was sensitive to interactions with small molecules. It has been well documented that groove binding and electrostatic interaction of small molecules show less or no perturbation on the base stacking and helicity bands, whereas intercalation alters the intensities of both the bands significantly, thus stabilizing the right-handed B conformation of DNA. The CD spectrum of ctDNA with the increasing concentrations of **8m** was shown in Fig. 9. As it can be observed

that upon addition of compound **8m**, CD spectrum was significantly perturbed. The ellipticity of both positive and negative band changed upon addition of compound **8m** to ct-DNA revealing conformational changes and base stacking within the DNA molecule. Thus the observed result supported an intercalative mode of binding. All the CD spectra were recorded in the range of 200-350 nm at a scan speed of 50 nm/min [48].

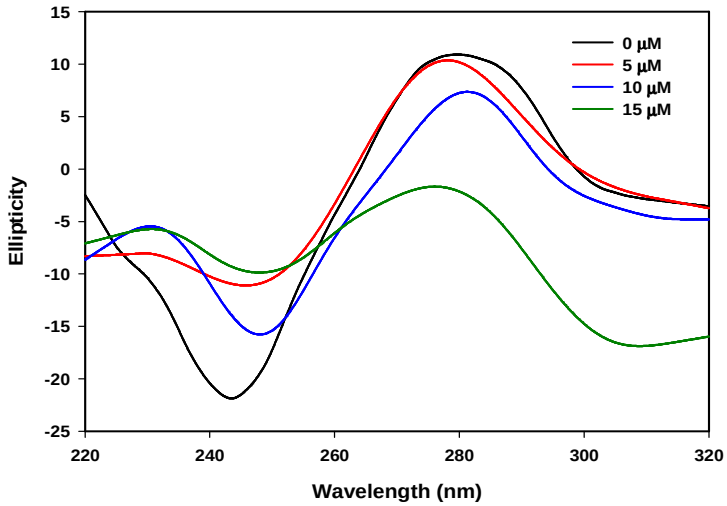

Fig. 9. Circular dichroism spectra of ctDNA with increasing concentrations of **8m**.

3.6.5. Molecular docking studies

The validity of docking protocol employed here was confirmed by performing re-docking of the ligand (HOECHST-33258) present in the X-ray crystal structure and comparing the RMSD between the docked pose and crystal structure pose. Supplementary Fig. S40 shows the binding of ligand at the minor groove of DNA as present in the X-ray structure and as predicted by molecular docking. The RMSD between the two poses was found to be 0.8356 Å, which is much lower than the allowed limit of 2.0 Å, confirming the validity of the adopted docking protocol.

To further evaluate the nature of the interaction of the lead compound with DNA, molecular docking studies were performed with the DNA dodecamer duplex of sequenced (CpGpCpGpApApTpTpCpGpCpG) (PDB ID: 8BNA). The best docking pose of compound **8m** with low energy (-9.9 kcal mol^{-1}), corresponding to a binding affinity of 1.82×10^7 M^{-1}) is presented in Fig. 11. The compound is interacting within the minor groove of DNA when combined with additional H-bonding interaction facilitates better DNA binding [49]. For comparative analysis, we also performed docking of a known minor groove binder

(HOECSHT-33258) to the dodecameric DNA molecule. Supplementary Fig. S41 shows the binding of HOECSHT-33258 at the minor groove of DNA. The structure was stabilized by two hydrogen bonds between N1 and N4 of HOECSHT-33258 with DT7 and DT8 of dodecameric DNA. The docking energy and binding affinity of HOECSHT-33258 towards DNA was estimated to be -11.6 kcal mol^{-1} and 3.22 × 10^{8} M^{-1}, respectively. It is worth to note that the binding affinity of **8m** was at least 10-folds higher the known minor groove binder, HOECSHT-33258.

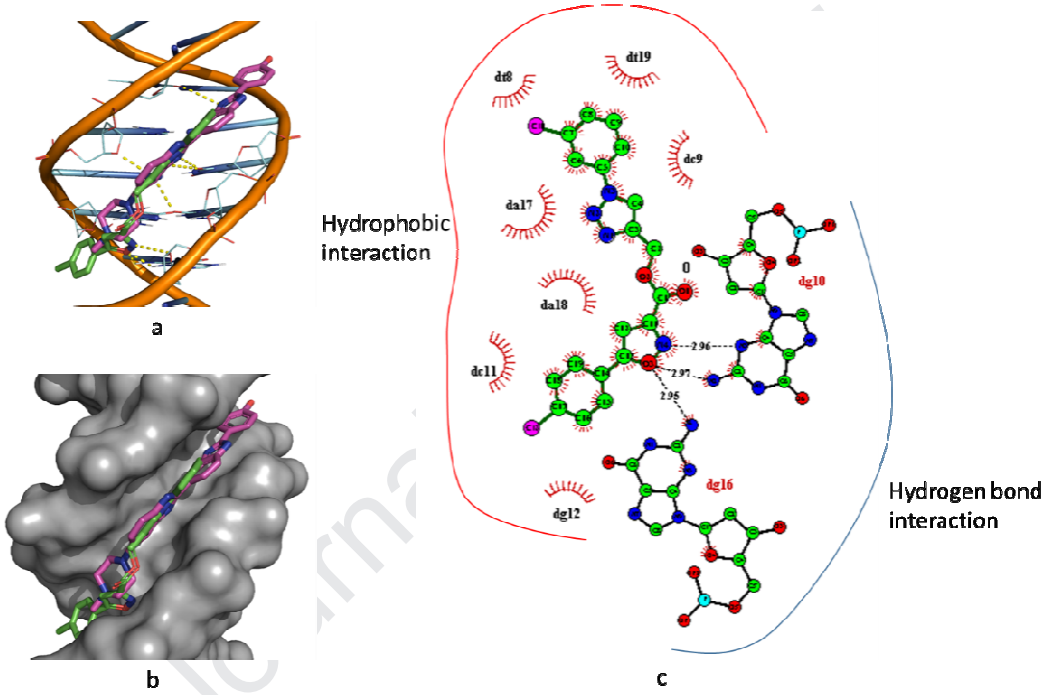

Fig. 10. *In silico* studies of lead compound **8m** with DNA dodecamer (PDB ID: 8BNA). Docking pose of compound **8m** along with reference compound HOECSHT-33258 showing interaction with DNA dodecamer in (a) cartoon image; (b) surface image. (c) LigPlot image showing hydrophobic interactions as well as hydrogen bond interaction with dg-10 and dg16 residue of DNA dodecamer.

4. Conclusion

To summarize, a series of isoxazole-triazole conjugates (**8a-q**) was synthesized by 1,3-cycloaddition reaction approach. Amongst all, **8b** and **8m** exhibited better antibacterial activity towards particular bacterial strains and showed no cytotoxicity against human cells (HEK293) even at higher concentrations. Compound **8m** showed significant inhibition potential against *E. coli* biofilm formation. Compound **8m** was further evaluated for DNA

binding ability to probe its possible mode of action. Various spectroscopic, electrochemical further corroborated with the experimental results. Our results suggested that the compound **8m** provide a suitable core for lead optimization and further pharmacological studies.

Conflict of interest

All authors declare no conflict of interest.

Acknowledgements

Farhat Habib acknowledges the financial support from University Grants Commission (UGC), Govt. of India in the form of non-NET Fellowship. The author would like to extend their sincere appreciation to the Deanship of Scientific Research at King Saud University, Riyadh, Saudi Arabia for funding this research group No. RGP-150.

References

[1] Doshi, H., Thakkar, S., Khirsariya, P., Thakur, M., Ray, A. 2015. 6-Tosyl-4,5,6,7-tetrahydrothieno [2,3-c] pyridine-3-carboxamide analogues: synthesis, characterization, MO calculation, and antibacterial activity. Appl. Biochem. Biotechnol. 175, 1700–1709.

[2] Review on Antimicrobial Resistance. Tackling drug Resistant Infections Globally: Final Report and Recommendations; May 2016.

[3] Li, B., and Webster, T.J. 2018. Bacteria Antibiotic Resistance: New challenges and opportunities for implant-associated orthopaedic infections. J. Orthop Res. 36(1), 22–32.

[4] Infectious Disease Society of America 2010. The 10 x 20 initiative pursuing a global commitment to develop 10 new antibacterial drugs by 2020, Clin. Infect. Dis. 50, 2081−2083.

[5] Peterson, J.W. Bacterial pathogenesis. In Medical Microbiology. 4th edition. University of Texas Medical Branch at Galveston, Texas, 1996.

[6] Bjarnsholt, T. 2013. The role of bacterial biofilms in chronic infections. Apmis. 121, 1-58.

[7] Hall-Stoodley, L., Costerton, J.W., Stoodley, P. 2004. Bacterial Biofilms: From the Natural Environment to Infectious Diseases. Nat. Rev. Microbiol. 2, 95−108.

[8] Arciola, C.R., Campoccia, D., Speziale, P., Montanaro, L., Costerton, J.W. 2012. Biofilm Formation in *Staphylococcus* implant infections. A Review of molecular mechanisms and implications for biofilm-resistant materials. Biomaterials. 33, 5967−5982.

[9] Jamal, M., Wisal, A., Saadia, A., Fazal, J., Muhammad, I., Muhammad, A.N., Tahir, H., Muhammad, A., Muhammad, R., Muhammad, A.K. 2018. Bacterial biofilm and associated infections. J. Chin. Med. Assoc. 81:1, 7–11.

[10] Dua, R., Shrivastava, S., Sonwane, S.K., Srivastave, S.K. 2011. Pharmacological significance of synthetic heterocycles scaffold: A Review. Adv. Biol. Res. 5(3), 120-144.

[11] Tarawneh, H., Al-Momani, L.A., Leon, F., Jain, S.K., Gadetskaya, A.V., Abu-Orabi, S.T., Tekwani, B.L., Cutler, S.J. 2018. Evaluation of triazole and isoxazole derivatives as potential antiinfective agents. Med. Chem. Res. 4, 1269–1275.

[12] Tariq, S., Alam, O., Amir, M. 2017. Synthesis, anti-inflammatory, p38α MAP kinase inhibitory activities and molecular docking studies of quinoxaline derivatives containing triazole moiety. Bioorg. Chem. 76, 343–358.

[13] Montes, G.C., M da Silva, B.N., Rezende, B., Sudo, R.T., Ferreira, V.F., Carvalho-da Silva, F., et al. 2017. The hypnotic, anxiolytic, and antinociceptive profile of a novel μ-opioid agonist. Molecules. 22(5), 800.

[14] Kaur, R., Dwivedi, A.R., Kumar, B., Kumar, V. 2016. Recent developments on 1,2,4-triazole nucleus in anticancer compounds: a review. Anti-Cancer Agents Med. Chem. 16, 465–489.

[15] Park, H.I. 2017. 1,2,3-triazole derivatives as antidiabetic agent, and methods for the preparation thereof, Korean Patent, Pham NTA, , 2017045941 A20170428.

[16] Chelamalla, R., Makula, A., Manda, S. 2017. Design, synthesis and *in silico* studies of new 5-substituted-2-(2-(5-aryl-1H-1,2,4-triazole-3-ylthio)acetyl) hydrazine carbothioamide/ carboxamides for anticonvulsant activity. Lett. Drug Des. Discov. 14, 1155–1163.

[17] Ashok, D., Gundu, S., Aamata, V.K., Devulappaly, M.G., Bathini, R., Manga V. 2018. Dimers of coumarin-1,2,3-triazole hybrids bearing alkyl spacer: design, microwave-assisted synthesis, molecular docking and evaluation as antimycobacterial and antimicrobial agents. J. Mol. Struct. 1157, 312–321.

[18] Cao, X., Wang, W., Wang, S., Bao, L. 2017. Asymmetric synthesis of novel triazole derivatives and their in vitro antiviral activity and mechanism of action. Eur. J. Med. Chem. 139, 718–725.

[19] Keivanloo, A., Bakherad, M., Abbasi, F., Sedani, T. B., Amin, A. H. 2016. Efficient synthesis of novel 1,2,3-triazole-linked quinoxaline scaffold via copper-catalyzed click reactions. RSC Adv., 6(107), 105433–105441.

[20] Kumar, S.S., Kavitha, H.P. 2013. Synthesis and biological applications of triazole derivatives. Mini-Rev. Org. Chem. 10(1), 40–65.

[21] Hua, F., Szostak, M. 2015. Recent Developments in the synthesis and reactivity of isoxazoles: Metal catalysis and beyond. Adv. Synth. Catal. 357, 2583–2614.

[22] Bibi, H., Nadeem, H., Abbas, M., Arif, M. 2019. Synthesis and anti-nociceptive potential of isoxazole carboxamides derivatives. BMC Chemistry. 13(6), 6.

[23] Kumar, R.N., Dev, G.J., Ravikumar, N., Swaroop, D.K., Debanjan, B.,Bharath, G., Narsaiah, B., et.al. 2016. Synthesis of novel triazole/isoxazole functionalized 7-(trifluoromethyl) pyrido[2,3-d]pyrimidine derivatives as promising anticancer and antibacterial agents. Bioorg. Med. Chem. Lett. 26(12), 2927-2930.

[24] Bustos, C., Molins, E., Carcamo, J.G., Aguilar, M.N., Sanchez, C., Villoslada, I.M., et. al. 2015. New 3,4,5-trisubstituted isoxazole derivatives with potential biological properties. New J. Chem. 39(6), 4295-4307.

[25] Wani, M.Y., Ahmad, A., Sheikh, R. A., Al-Ghamdi, K.J., Sobral, A.J.F.N. 2015. Imidazole clubbed 1,3,4-oxadiazole derivatives as potential antifungal agents. Bioorg. Med. Chem. Lett. 23(15), 4172-4180.

[26] Dheer, D., Singh, V., Shankar, R. 2017. Medicinal attributes of 1,2,3-triazoles: Current developments. Bioorg. Chem. 71, 30–54.

[27] Masood, M.M., Pillalmarri, V.K., Irfan, M., Aneja, B., Jairajpuri, M.A., Zafaryab M., et al. 2015. Diketo acids and their amino acid/dipeptidic analogues as promising scaffolds for the development of bacterial methionine aminopeptidase inhibitors. RSC Adv. 5(43), 34173-34183.

[28] Hasan, P., Pillalmarri, V.K., Aneja, B., Irfan, M., Azam, M., Perwez, A., et al. 2019. Synthesis and mechanistic studies of diketo acids and their bioisosteres as potential antibacterial agents. Eur. J. Med. Chem. 163, 67–82.

[29] Najafi, Z., Mahdavi, M., Safavi, M., Saeedi, Mina.,Alinezhad, H., Pordeli, M., et al. 2015. Synthesis and *in vitro* cytotoxic activity of novel triazole-isoxazole derivatives. J. Heterocycl. Chem. 52(6), 1743–1747.

[30] Aneja, B., Azam, M., Alam, S., Perwez, A., Maguire, R., Yadav, U. et al. 2018. Natural product-based 1,2,3-triazole/ sulfonate analogues as potential chemotherapeutic agents for bacterial infections. ACS Omega. 3, 6912−6930.

[31] Nayab, P.S., Pulaganti, M., Chitta, S.K., Abid, M., Uddin, R. 2015. Evaluation of DNA binding, radicals scavenging and antimicrobial studies of newly synthesized *N*-substituted naphthalimides: spectroscopic and molecular docking investigations. J. Fluoresc. 25(6), 1905–1920.

[32] War, J.A., Srivastava, S.K., Srivastava, S.D. 2017. Design, synthesis and DNA-binding study of some novel morpholine linked thiazolidinone derivatives. Spectrochim. Acta A. 173, 270–278.

[33] Jumbri, K., Ahmad, H., Abdulmalek, H.E., Rahman, B.A. 2016. Binding energy and biophysical properties of ionic liquid-DNA complex: Understanding the role of hydrophobic interactions. J. Mol. Liq. 223, 1197–1203.

[34] Tahir, S., Badshah, A., Hussain, R.A., Tahir, M.N., Tabassum, S., Patujo, J.A., et al. 2015. DNA-binding studies and biological activities of new nitrosubstituted acyl thioureas. J. Mol. Struct. 1099, 215–225.

[35] DeLano, W. 2002. The PyMOL user's manual. DeLanoSci San Carlos, CA.

[36] (a) Huang, S., Song, C., Wang, X., Zhang, G., Wang, Y., Jiang, X., Sun, Q., Huang, L., Xiang, R., Hu, Y., Li, L. 2017. Discovery of new SIRT2 inhibitors by utilizing a consensus docking/scoring strategy and structure–activity relationship analysis. *J.* Chem. Inf. Model. 57(4), 669-679. (b) Wang, J.L., Li, L., Hu, M.B., Wu, B., Fan, W.X., Peng, W., Wei, D.N., Wu, C.J. 2019. *In silico* drug design of inhibitor of nuclear factor kappa B kinase subunit beta inhibitors from 2-acylamino-3-aminothienopyridines based on quantitative structure–activity relationships and molecular docking. Comput. Biol. Chem. 78, 297-305.

[37] (a) Rehman M.T, Al-Ajmi M.F., Hussain A, Rather G.M., Khan M.A. 2019. High-throughput virtual screening and Molecular dynamics simulation identified ZINC84525623 a potential inhibitor of NDM-1. Int. J. Mol. Sci. 20, 819. (b) Rehman, M.T., Shamsi, H., Khan, A.U. 2014. Insight into the binding mechanism of imipenem

to human serum albumin by spectroscopic and computational approaches. Mol. Pharm. 11, 1785–1797.

[38] Masood, M.M., Pillalamarri, V.K., Irfan, M., Aneja, B., Jairajpuri, M. A., Zafaryab, M., Rizvi, M. M. A., Yadava, U., et. al. 2015, Diketo acids and their amino acid/dipeptidic analogues as promising scaffolds for the development of bacterial methionine aminopeptidase inhibitors, RSC Adv. 5, 34173.

[39] Irfan, M., Aneja, B., Yadav, U., Khan, S.I., Manzoor, N., Daniliuc, C.G., et al., 2015. Synthesis, QSAR and anticandidal evaluation of 1,2,3-triazoles derived from naturally bioactive scaffolds. Eur. J. Med. Chem. 93, 246-254.

[40] Khan, P., Rahman, S., Queen, A., Manzoor, S., Naz, F., Hasan, G.M. et al. 2017. Elucidation of dietary polyphenolics as potential inhibitor of microtubule affinity regulating kinase 4: *in silico* and *in vitro* studies. Sci. Rep. 7(1), 9470.

[41] Zimmermann, L.A., Moraes de, M.H., Rosa da, R., Meloc de, B.E., Paulad, F.R., Eloir P. Schenkela, P.E., et al. 2018. Synthesis and SAR of new isoxazole-triazolebis-heterocyclic compounds asanalogues of natural lignans with antiparasitic activity. Bioorg. Med. Chem. 26, 4850–4862.

[42] Yang, Z.S., Yan-Ling, W., Zhao, G.C. 2004. The interaction of copper-bipyridyl complex with DNA and cleavage to DNA. Anal. Sci. 20(8), 1127–1130.

[43] Song, Y.H., Yoo, C.M., Hong, A.P., Kim, S.H., Jeong, H.J., Shin, S.Y. 2008. DNA-Binding study identifies C-Box and hybrid C/G-box or C/A-box motifs as high-affinity binding sites for STF1 and long hypocotyl5 Proteins. Plant Physiol. 146, 1862–1877.

[44] Aravinda, T., Naik, H.S.B., Naik, H.R.P. 2009. 1, 2, 3-Triazole fused quinoline-peptidomimetics: Studies on synthesis, DNA binding and photonuclease activity. Int. J. Pept. Res.15, 273.

[45] Sharath, N., Naik, H.S.B., Kumar, B.V. 2012. Synthesis, DNA binding, and photonuclease activity of new tetraazamacrocyclic constrained isoxazole rings as subunit in metal complexes. Nucleosides Nucleotides Nucleic Acids, 31(11), 813–829.

[46] Babu, B., Brien, K.A., Satam, V., Plaunt, A., Pressler, M., Shen, H., et al. 2012. Synthesis and DNA-binding properties of 1,2,3-triazole-linked H-pin pyrrole- and imidazole-containing polyamides formed by the Huisgen reaction. Heterocycl. Commun. 18(2), 79–85.

[47] Sarwar, T., Husain, M.A., Rehman, S.U., Ishqi, H.M., Tabish, M. 2015. Multi-spectroscopic and molecular modelling studies on the interaction of esculetin with calf thymus DNA. Mol. BioSyst. 11(2), 522–531.

[48] Sarwar, T., Husain, M.A., Rehman, S.U., Ishqi, H.M., Tabish, M. 2015. Multi-spectroscopic and molecular modelling studies on the interaction of esculetin with calf thymus DNA. Mol. BioSyst. 11(2), 522–531.

[49] Arif, R., Amaduddin, Ahmed, S., Ahmed, S., Abid, M. 2018. Synthesis, *in vitro* biological evaluation and *in silico* studies of some new heterocyclic Schiff bases. Chemistry Select. 3, 13517– 13525.

Highlights

- Novel isoxazole-1,2,3-triazole conjugates (**8a-q**) were synthesized and confirmed by multi spectroscopic analysis.
- *In vitro* antibacterial screening against various bacterial strains showed compound **8m** as potential lead inhibitor.
- Cytotoxicity assay on HEK293 cells showed non-toxic nature of the lead compound.
- XTT assay and SEM analysis confirmed that compound **8m** significantly inhibited biofilm formation.
- DNA binding studies of **8m** showed intercalating mode of binding.